Pattern Formation in Icosahedral Virus Capsids: The Papova Viruses and Nudaurelia Capensis β Virus

Christopher J. Marzec and Loren A. Day
Public Health Research Institute, New York, New York 10016 USA

ABSTRACT The capsids of the spherical viruses all show underlying icosahedral symmetry, yet they differ markedly in capsomere shape and in capsomere position and orientation. The capsid patterns presented by the capsomere shapes, positions, and orientations of three viruses (papilloma, SV40, and NβV) have been generated dynamically through a bottom-up procedure which provides a basis for understanding the patterns. A capsomere shape is represented in two-dimensional cross-section by a mass or charge density on the surface of a sphere, given by an expansion in spherical harmonics, and referred to herein as a morphological unit (MU). A capsid pattern is represented by an icosahedrally symmetrical superposition of such densities, determined by the positions and orientations of its MUs on the spherical surface. The fitness of an arrangement of MUs is measured by an interaction integral through which all capsid elements interact with each other via an arbitrary function of distance. A capsid pattern is generated by allowing the correct number of appropriately shaped MUs to move dynamically on the sphere, positioning themselves until an extremum of the fitness function is attained. The resulting patterns are largely independent of the details of both the capsomere representation and the interaction function; thus the patterns produced are generic. The simplest useful fitness function is Σ^2, the average square of the mass (or charge) density, a minimum of which corresponds to a "uniformly spaced" MU distribution; to good approximation, the electrostatic free energy of charged capsomeres, calculated from the linearized Poisson-Boltzmann equation, is proportional to Σ^2. With disks as MUs, the model generates the coordinated lattices familiar from the quasi-equivalence theory, indexed by triangulation numbers. Using fivefold MUs, the model generates the patterns observed at different radii within the $T = 7$ capsid of papilloma and at the surface of SV40; threefold MUs give the $T = 4$ pattern of Nudaurelia capensis β virus. In all cases examined so far, the MU orientations are correctly found.

INTRODUCTION

Determinations of the capsid structures of the spherical viruses have revealed a great variety of patterns, virtually always following an underlying icosahedral symmetry. A capsid "pattern" is given by the shapes, positions, and orientations of its capsomeres, which are capsid structural units typically composed of one to six individual protein subunit monomers; the centers of the capsomeres lie on a "lattice," a more limited notion which excludes anything to do with capsomere shape. The well-known triangulation numbers T, used to index these lattices, have been assigned for many viruses, and for several viruses the structures are known either to atomic resolution or to sufficient resolution to reveal details of the capsid pattern, on a nanometer distance scale. Some viruses contain only a single type of capsid protein subunit, organized into either a single type of capsomere or into two types (pentamers and hexamers), whereas other capsids are composed of two or more major coat protein subunits and several minor proteins, such as spike proteins that extend well beyond the outer capsid layers or proteins that extend inwardly from the capsid. The individual major protein subunits range in copy number from 60 to several thousand, and in molecular weights from ~10,000 to more than 100,000. Some capsomeres with fivefold symmetry are almost round at some radii, yet pentagonal and star-like at other radii, such as in the papovaviruses (polyoma, SV40, and papilloma) (Rayment et al., 1982; Rayment, 1985; Baker et al., 1988, 1989, 1991; Liddington et al., 1991). Nudaurelia capensis β virus (NβV) has a capsomere with threefold symmetry, with about two-thirds of its mass in an open trefoil "Y" shape at an outer radius and the remaining one-third of its mass at an inner radius, with a rounded triangular shape (Olson et al., 1990). Likewise, the hexon capsomere of adenovirus, made of three subunits, is a triangular tower at outer radii and a hexagonal cone at inner radii (Burnett, 1985). This paper argues that such capsid patterns can be understood as packing arrangements induced by the shapes of the capsomeres; the connection is demonstrated explicitly for the papovaviruses and for NβV.

The classical paper by Crick and Watson (1956), which first discussed the general requirement for high symmetry in virus structures, and the papers of Horne and Wildy (1961) and Caspar and Klug (1962) all observed that the capsids are made of many identical copies of proteins that are the products of either one or a small number of genes. Horne and Wildy considered the symmetrical capsomere to be the primary structural unit of the capsids of the spherical viruses, situating the capsomeres at the vertices of lattices which can be enumerated by requiring consistency with the fundamental icosahedral symmetry. The same lattices appear in the quasi-equivalence theory of Caspar and Klug (1962), built around relations among the protein subunits. Quasi-equivalence confronts the geometrical constraint that, except for the virus particles with true $T = 1$ symmetry and 60 subunits (Liljas et al., 1982), there is no way to cover a closed

Received for publication 8 February 1993 and in final form 22 September 1993.

Address reprint requests to either author at the Public Health Research Institute, 455 First Avenue, New York, NY 10016.

0006-3495/93/12/2559/19 $2.00

surface with many copies of one protein subunit so that all subunits have an identical physical-chemical environment. Given this geometrical mandate for differences, the fundamental, mechanistic assumption of quasi-equivalence was about how to reconcile them, with minimum energy cost.

The theoretical construction of quasi-equivalence is obtained in two steps. First, one considers a Platonic solid, with its surface "coordinated" in the manner first used by Goldberg (Goldberg, 1937), i.e., covered by a regular, trigonal lattice parametrized by two integers, m and n, related to the triangulation number:

$$T = m^2 + mn + n^2. \quad (1)$$

Caspar and Klug noted that T is the number of facets of the trigonal lattice per face; a facet can extend across an icosahedron edge to lie on two of its faces, but each face contains an integral number of facets, when the complete and fractional facets are added up (Caspar and Klug, 1962; see also Casjens, 1985). Second, into each facet triangle of this lattice one sets three subunits, each of which bonds chemically to its immediate neighbors. The majority of the vertices are hexavalent, surrounded by six subunits, but the vertices of the Platonic solid are surrounded by a smaller number of subunits. Thus the tetrahedron has 4 trivalent vertices, the octahedron has 6 tetravalent vertices, and the icosahedron has 12 pentavalent vertices. Quasi-equivalence postulates that the best capsid structure is one arranged so that the necessary deviations from some one optimal bonding pattern cost minimum energy; this is the assumption of quasi-equivalent bonding. Tarnai and Gaspar (1987), referring to the quasi-equivalence theory, mention its "local extrema arrangements." Because the nearest neighbor interactions of hexavalent subunits are more similar (quasi-equivalent) to nearest neighbor interactions of pentavalent subunits than they would be to those of tetravalent or trivalent subunits, the constraint of quasi-equivalent bonding selects the icosahedron. The icosahedron possesses 20 faces, and its symmetry axes pass through 12 fivefold centers (the pentavalent vertices), 20 threefold centers, and 30 twofold centers; the coordinated icosahedron has $10T + 2$ vertices altogether. The quasi-equivalent bonding pattern required by this reasoning leads inexorably to hexamers positioned at $10(T - 1)$ vertices of the coordination lattice, which are the local "quasi sixfold" symmetry centers, and pentamers at the 12 fivefold vertices. This is equivalent to the prediction that the capsid must contain 3 (subunits per facet) $\times$ T (facets per face) $\times$ 20 (faces) = $60T$ subunits altogether.

Some virus capsids are numerically consistent with quasi-equivalence: the $T = 3$ plant viruses, with the predicted 180 copies of identical subunits (Harrison et al., 1978; Olson et al., 1983; Rossmann and Erickson, 1985; Rossmann and Johnson, 1989); the $T = 4$ viruses Nudaurelia capensis β virus (Olson et al., 1990) and bacteriophage P4 (Dokland et al., 1992), with 240 subunits; the $T = 7$ bacteriophages, including P2, related to P4 (Dokland et al., 1992), P22 (Casjens, 1979; Prevelige et al., 1988), λ (Katsura, 1983), and HK97 (R.W. Hendrix, University of Pittsburgh, personal communication), all with the predicted 420 copies of their major capsid protein save the few replaced by portal proteins of the tail assembly; and cauliflower mosaic virus, which has 420 identical subunits (Cheng et al., 1992). However, scrutiny of structures for which high-resolution data are available shows that the degree and type of bond-deformation posited by quasi-equivalence does not occur, and that the different types of bonding required by subunit positions on the lattice are satisfied by different, non-quasi-equivalent bonds (Olson et al., 1983; Burnett, 1985; Rossmann and Erickson, 1985; Olson et al., 1990).

Furthermore, it is now generally recognized that the $T = 7$ virus polyoma (Rayment et al., 1982; Rayment, 1985), and the related viruses SV40 (Baker et al., 1988; Baker et al., 1989; Liddington et al., 1991) and papilloma (Baker et al., 1991) provide counterexamples to the numerical predictions of quasi-equivalence. They contain pentamers at all $10T + 2 = 72$ vertices, for a total of 360 subunits; quasi-equivalence predicts hexamers at each of the $10(7 - 1) = 60$ local sixfold centers and 60 subunits at the vertices, for a total of 420 subunits. Further, in the $T = 25$ adenovirus, the 240 capsomeres at the local sixfold centers are trimers of subunits, not hexamers, and the 12 fivefold centers are occupied by a different protein altogether (Burnett, 1985).

An important aspect of the counterexamples to quasi-equivalence is that the 60 unexpected pentamers in the papovaviruses are at the 60 positions on the standard $T = 7$ lattice predicted for hexamers, and likewise the 240 trimers in adenovirus are at capsomere positions on the standard $T = 25$ lattice, namely the hexavalent positions of these lattices. We are left with the paradox that the large-scale taxonomic part of quasi-equivalence, the appearance of coordination lattices indexed with T values, appears valid universally, yet neither the small-scale taxonomy of subunit numerology nor the theoretical rationalization in terms of quasi-equivalent bonding holds.

We believe that the resolution to the paradox is in the unsung core of the Caspar-Klug theory, beneath the chemistry of bonding patterns. This is the assumption that the correct structures show a minimum in the distortion of an optimum pattern, given the global constraint of covering a more-or-less spherical surface. Quasi-equivalence implicitly acknowledges that the coordinated surface lattices must somehow engender a minimum of some major component of the capsid free energy. Subsequent data has shown that the choice to minimize bond deformation energy was incorrect. Accordingly, we replace bond deformation energy with a more general measure of the global capsid self-interaction, which we will denote by E_{INT}, discussed below.

In this paper, we take the icosahedral symmetry as a given and focus on understanding the patterns observed within that symmetry. The patterns are two-dimensional, existing on the roughly spherical surface of an icosahedral virus or on a spherical section through a capsid. Therefore, our model represents the cross-sections of the capsomeres which contribute to the pattern as two-dimensional objects and allows them to wander on the spherical surface. They position themselves as

an autonomous, dynamic system, i.e., without any nudges from the programmer, to seek out a local minimum (or extremum) in E_{INT}. Thus our model avoids putting in the capsid positions by hand, as done by Horne and Wildy (1961) and by Caspar and Klug (1962). Furthermore, in the two cases which we have examined so far in which the capsomere cross-section is distinctly nonround (papovaviruses and NβV), we have found that the orientations of the capsomeres are also correctly generated.

Our goal in this paper is not to present an assembly model, but to rationalize observed capsid patterns. We believe that this can be achieved by appealing to features which a complete model must have, even though a complete model is not available. The work of Salunke et al. (1989) on the polymorphism of polyoma VP_1 subunit assemblies offers a physical picture from which to begin. They showed that electrostatic effects switch assembly into icosahedrally symmetrical shells with $N = 72$ capsomeres, into smaller octahedrally symmetrical shells with $N = 24$, into still smaller icosahedrally symmetrical shells with $N = 12$, or into cylindrical sheets. They conjectured that solvent conditions which increase the negative charge on the capsomere surfaces cause the radius of the assembling shell to decrease, because the greater angular separation of capsomeres, due to smaller N, results in greater separation of the repelling charges. Implicit in their argument is a radial balance between the repelling electrostatic force and an unspecified, but necessary, attractive force; because of the shell curvature, all forces between capsomeres possess radial components. Their argument also requires that the negative charges are located near the outer portion of the capsomere; otherwise, if the charges were located at the nominal shell radius, where the capsomeres are packed shoulder to shoulder, changes in the radius would not alter the distance between the repelling charges. Thus, the radial component of the repelling force balances the radial attractive force, but its tangential component causes a distance-dependent mutual capsomere repulsion, a pressure, in the outer portions of the capsid. So we can ask what patterns are formed by the outer layers of the capsid as they arrange themselves to minimize the capsid average of this repulsive potential energy. To render this question tractable, we reduce the capsomere to its two-dimensional cross-section at a radius R and consider how N such cross-sections can space themselves while moving on the surface of a sphere of this radius. The attractive force is present in the modeling as the mechanism which constrains the motion to the surface of the sphere. We proceed on the assumption that these considerations are general and will apply with appropriate modification to many or most capsids; the repelling force can be due to hydration; the attractive force can be hydrophobic or electrostatic, involving condensation around the nucleic acid.

OPTIMAL COVERINGS OF THE SPHERE FROM NONSPECIFIC INTERACTIONS

The mathematical problem of distributing objects on the sphere has had many incarnations, and it confers much insight into our biological question of pattern formation vis-a-vis capsomere interaction. The Tammes "packing" problem (Tammes, 1930) is to find the closest packing of N hard spheres on a spherical surface, and it can be rephrased as how to distribute N points on the sphere so as to maximize the smallest distance between them (Tarnai and Gaspar, 1987). Goldberg (1967) first stated the connection between virus structure and the Tammes problem. Melnyk et al. (1977) noted that the Tammes problem is equivalent to minimizing the field energy of N points on the sphere, interacting through an inverse power law ($V = r^{-n}$) potential, as the power becomes arbitrarily large, thus penalizing most severely the closest points. Clare and Kepert (1986) also spaced points on a sphere using an inverse power potential in the large n limit. It is found in general that for most values of N, the best packing arrangements have little or no apparent symmetry, but that for some N values, the best packing shows the symmetry of the Platonic solids with the spheres or points near the vertices of a coordination lattice (Tarnai and Gaspar, 1987). For example, Clare and Kepert (1986) found that the optimum packing for 32 hard spheres is very close to icosahedral. Tarnai and Gaspar (1987) have extended the range of N for which optimum packings of hard spheres are known, basing their approach on triangulations of underlying Platonic solids. These studies of the Tammes problem offer a clue about the nature of the global interaction measured by E_{INT}; both long-range interactions like the potential fields with moderate n values, and short-range interactions, like the packing of hard, impenetrable spheres, serve to construct essentially the same patterns.

The Tammes packing problem and its mathematically precise relatives do not map directly onto the problem of virus capsid structure. Tarnai (1991) notes that the related Tammes "covering" problem seems empirically to be of more relevance to capsid structures. The covering problem asks how to arrange N overlapping disks of the smallest possible diameter, so as to completely cover a sphere. Biological structures have soft edges blurred by thermal motion and typically interact through solvent-mediated mechanisms; biological structures simply do not look much like systems of hard spheres, or of points interacting through a field. The overlapping disks used by the Tammes covering problem afford a closer match to the biological problem than do the hard disks of the packing problem, and this is built into the formalism developed below for representing the capsomeres. But despite their great differences, the Tammes problems and the capsid pattern morphogenesis problem spawn similar patterns. This fact is telling, suggesting that in both systems the patterns are created by nonspecific interactions.

The polymorphism of structures assembled from polyoma VP_1 protein has been mentioned above; the Tammes problem also shows polymorphism, in that different numbers of points or disks pack on the sphere with maximum efficiency when they show different Platonic symmetries, or, for some N, no apparent symmetry. Liddington et al. (1991) have shown that

each SV40 pentamer has five flexible COOH-terminal arms, which they expect to be "flexible and unstructured on a free pentamer," and which bond noncovalently to arms from neighboring pentamers, flexing to accommodate the different local capsomere environments; they make a mechanical metaphor likening the bonding arms to ropes, rather than cement. They note that although the arms interact with each other via "precise contacts in the target subunit," they must do this "without imposing strong restrictions on symmetry." If a specific interaction is one which fixes structure by virtue of its specificity, then the bonding arms of SV40 represent a new sort of nonspecific interaction, their precise contacts notwithstanding, because the flexibility of the rope-like bonding arms serves only to fix a maximum distance between bonded pentamers, rather than to induce a mutual orientation. The bonding arms of SV40 are visible in a cryoelectron microscropy reconstruction made by Baker et al. (1988), and Baker et al. (1991) commented extensively upon similar intercapsomere structures in the papilloma capsid, one originating in each subunit. Thus, even in papovaviruses SV40 and papilloma, Platonic symmetry evidently arises from some nonspecific mechanism acting between capsomeres made of VP_1 protein subunits, and we find it plausible that nonspecific mechanisms also determine the structures of polyoma VP_1 assemblies not possessing Platonic symmetry. Accordingly, as a working hypothesis, we have assumed that, like the global capsid symmetry itself and the patterns found in the Tammes problem studies, the capsid patterns possible for a given capsomere are also determined by nonspecific interactions.

THE REPRESENTATION

To avoid the rigidity of the Tammes packing problem and to include the inherent uncertainty in capsomere position due to thermal effects, we represent the capsomeres and their interactions by continuous functions. This avoids hard sphere capsomeres which interact only if in direct contact. We will denote a modeled capsomere as a morphological unit, an "MU." An MU is to be thought of as an abstracted capsomer, containing only the minimum information about its shape needed to determine the capsid pattern, representing the shape of the capsomere as seen in its capsid, notwithstanding possible shape changes which might occur during virus assembly. In accord with the discussion above relating the forces acting on the capsid outer layers to features of a full-assembly model, we represent the capsid as the surface of a sphere, and our MUs are two-dimensional spherical caps, polygons, or more general shapes. Giving the capsomere a nonround shape is necessary for studying a virus such as papilloma, with capsomeres having strong fivefold symmetry.

The MUs are conveniently written by Fourier expansion in spherical harmonics. (This is the analogue in spherical geometry of Fourier expansion via sines and cosines in rectilinear geometry; the trigonometric functions and the spherical harmonics are solutions of the Laplace equation, written in rectilinear or spherical coordinate systems, respectively.) Vogel and Provencher (1988) used spherical harmonics to represent capsid density for reconstructing projections of disordered virions. Thus

$$\sigma_{\mathrm{MU}}(\Theta, \phi) = \sum_{l=0}^{L} \sum_{m=-l}^{l} a_{lm} Y_{lm}(\Theta, \phi). \tag{2}$$

This σ_{MU} refers to an MU sitting on the north pole of a sphere, and Θ and ϕ are the usual spherical coordinates. The Appendix shows that the surface density of the entire icosahedrally symmetrical capsid can be written as

$$\begin{aligned} \sigma(\Theta, \phi) &= \sum_{l,m,m'} M^{l}_{m,m'}(\{R_j\}) a_{l,m'} Y_{lm}(\Theta, \phi) \\ &\equiv \sum_{l,m} c_{lm} Y_{lm}(\Theta, \phi), \end{aligned} \tag{3}$$

where matrix M is a function of the positions of the MUs. As in the Appendix, we label the position of the jth MU by R_j, which represents the rotation through Euler angles α_j, β_j, γ_j, that takes the north pole of the sphere to the position and orientation of the jth MU. Angles α_j and β_j are, respectively, the spherical ϕ and Θ coordinates of the jth MU. Angle γ_j is the rotation needed to orient the jth nonround MU about its local axis; it is unnecessary if the MU is round.

This representation has the constraint that its resolution is limited by the number of spherical harmonics which can be included, given by L. In practice, we can take $L = 50$. This affords a stable representation for fewer than about 500 MUs altogether, in that solutions are well-determined and do not change substantially if we choose $L = 49$ or $L = 51$. Because L is finite, the MU is necessarily somewhat fuzzier than the capsomere it models. This is qualitatively in accord with the fact that the capsomeres are not hard-edged.

To assert a general form for the interaction function, we assume that two patches on the capsid surface interact via the product of their masses, weighted by an arbitrary function of the distance r between them; e.g., if the interaction were gravitational, which it certainly is not, the interaction function would be $1/|r_1 - r_2|$. The total interaction is found by summing over all pairs of patches. Because the arc length between two points on a sphere of radius R equals $R\Phi$, where Φ is the angle between them, the interaction function can be written as $f(\Phi)$. Expanding in Legendre polynomials gives

$$f(\Phi) = \sum_{l=0}^{\infty} g_l P_l(\cos \Phi). \tag{4}$$

The interaction function is now completely characterized by the numbers g_l, and by choosing them appropriately, any function of distance on the sphere can be constructed.

The Appendix shows that the form of E_{INT}, given the assumptions above, is

$$E_{INT} = \sum_{l=0}^{L} \sum_{m=-l}^{l} w_l c_{lm} c^*_{lm}, \quad (5)$$

where $w_l \equiv 4\pi R^4 g_l/(2l + 1)$.

Once the a_{lm} (MU shape) and the w_l (interaction function) are specified, a solution to the MU spacing problem is a set of angles R_j which give positions of the MUs that correspond to a local minimum of E_{INT}. Because of the assumed icosahedral symmetry, only a small number of MUs are dynamically independent, the majority being symmetry projections of these. A steepest descent algorithm adjusts the startup set of the R_j to obtain progressively lower values of E_{INT} until the angular derivatives of E_{INT} are sufficiently small. At that point, to hasten convergence, the minimum is found by Newton-Raphson linearization of the solution equations $\partial E_{INT}/\partial \delta_k = 0$, where δ_k represents all of the Euler angles. Found via this last equation, a solution set of Euler angles gives an extremum of E_{INT}, which in general could be a maximum, minimum, or a saddle point. The kind of extremum is determined from the eigenvalues of the matrix $\partial^2 E_{INF}/\partial\delta_j\partial\delta_k$; solutions with all positive eigenvalues are stable, and the appearance of a negative eigenvalue indicates an unstable, saddle point solution. The stable solutions, corresponding to local minima and not in need of external stabilization, seem most easily applicable to capsid architecture. However, we discuss below the case of SV40, in which saddle point solutions do seem relevant.

GENERICITY IN SHAPE AND INTERACTION

Before using the apparatus discussed above to create capsid patterns, we need to choose definite values for the a_{lm} and the w_l of the interaction function. In this section we show that the patterns generated do not depend significantly on the details of our choices, as anticipated from the studies of the Tammes problem noted above. The emergence of the coordination lattices is referred to as "generic" because large changes in the input, in this case the distributions a_{lm} and w_l, cause only inconsequential changes in the output. Thus, for the purpose of understanding the origins of the patterns, it is enough that our choices for a_{lm} and w_l give only a qualitatively correct picture of the MU and its interactions.

As argued above, we suppose that the outer portions of a capsid in an equilibrium configuration can be modeled as constrained to the surface of a sphere, wherein they experience a mutual repulsion. We consider two different situations to show how repelling forces can easily arise.

The first physical model for the repelling interaction is presented in section II of the Appendix, which considers an interaction between charged MUs based on the linearized Poisson-Boltzmann equation and calculates w_l for this case. Here σ_{MU} measures charge density, and the minimized function is the Helmholtz free energy, $A \equiv E - TS$. We investigate this interaction because it is often used in structure investigations, it is mathematically tractable, and it can be tuned to give long-, medium-, or short-range interactions. The tuning is accomplished by varying the Poisson-Boltzmann damping factor, κ. Decreasing κR increases the range of the interaction, and as $\kappa R \to 0$, w_l approaches $2\pi R^3/(2l + 1)$, the Coulomb limit wherein the interaction is mediated by an undamped $1/|\vec{r} - \vec{r}'|$ field. The Coulomb limit gives the longest ranged interaction imaginable. As κR is increased, w_l approaches $\pi R^2/(\kappa\sqrt{\epsilon})$, independent of l. In this limit, the MUs feel each other only through immediate contact, the interaction mediated by a δ function. Evaluation of the expression in the Appendix shows that for $\kappa R > \approx 10$, the function w_l vs l is essentially flat, the long interaction limit. Because the capsid radius R is very large, typically several hundred Angstroms, the larger κR values and the short-range interaction are physically more relevant, but we would be hard-pressed to decide which value of κR is best on physical grounds. The value of κ depends on solvent conditions.

Our second, more qualitative, interaction picture invokes hydration forces between capsomere surfaces. Hydration forces have been measured for polysaccharides (Rau and Parsegian, 1990), DNA helices (Rau and Parsegian, 1992), and electrically neutral or charged phospholipid bilayers (Rand and Parsegian, 1989). Rau and Parsegian (1990) note that "hydration forces seem very probably a general and dominating feature of the interactions between all water-soluble surfaces at close approach." Hydration forces, due to structuring of water between interacting surfaces, can be either strongly attractive or repulsive, and for the high symmetry geometries experimentally accessible, they typically fall off exponentially, with a scale length of several Angstroms (Rau and Parsegian, 1990; Rau and Parsegian, 1992). The distance integral of the repulsive hydration force is an energy corresponding to a short-ranged interaction function $f(\Phi)$ between two surfaces; for the two-dimensional model, this becomes an integral over MU perimeters. Although the formalism leading to Equ. 5 entails integrating over MU areas, not perimeters, the short range of the hydration force means that elements of area in the interior of an MU would not interact strongly with similar elements of neighboring MUs; the double integral over MU area would in effect sum up contributions from the perimeters. Thus, an interaction based on the repulsion of hydrophilic surfaces again leads to the limiting case of a short-ranged interaction.

The choice of a_{lm} presents similar difficulties. The most straightforward model for a round MU is a hard-edged disk of radius a, whose density is constant for $r < a$, then falls immediately to zero for $r > a$. This has the disadvantage of producing oscillations in the density distribution, "ringing," for r just larger than a, which is decidedly nonphysical. The hard-edged disk also has the unattractive mathematical feature that its a_{lm} fall off very slowly, so the truncation for $l > L$ might be serious. Ringing can be avoided, and a smooth falloff of the a_{lm} can be assured, by modeling a round MU by a Gaussian. However, this form is also decidedly

nonphysical, because it would tend to exaggerate the range of the interaction.

In practice, we find that these various choices all lead to essentially the same solutions. Fig. 1 shows a superposition of six $T = 7$ models. These are made by choosing two forms for the interaction, applied to each of three forms for the MU. The interaction is given by the two limiting forms, $\kappa R = 0$ and $\kappa R = \infty$. Two of the MU forms are the hard and Gaussian disks described above; the third is a Gaussian profile pentagon, used to model papilloma as discussed below. We see that the solutions for the six models superimpose with only very marginal differences in the MU positions. Similar results apply to other T values. We conclude that in terms of MU shape and interaction, the models are essentially equivalent. Insofar as we are interested in understanding pattern formation and stability, we do not need to choose among the various prescriptions for modeling the MU and interaction on any basis but convenience. The same patterns arise because the minimization enforced by our dynamic scheme depends strongly on the MU positions and weakly on the details of the minimized function.

Because the various sorts of disks yield the same lattices, we have chosen MUs with a Gaussian radial profile, because of its convenient smoothness. Our method for constructing a nonround MU is simply to use a shape like the capsomeres in the capsid pattern which we are attempting to model. For a nonround MU situated at the north pole, the rate of falloff with polar angle Θ is a function of azimuthal angle ϕ, chosen so that the maximum rate of falloff corresponds to a contour level which traces out the nominal perimeter of the modeled capsomer (see the Appendix for details). Below we use pentagonal, star-shaped, and trefoil MUs.

It is useful to introduce the average of the square of the surface density of the mass, denoted Σ^2. The Appendix shows that Σ^2 appears as a special, simple case of interaction integral E_{INT} by setting $w_l = 1/4\pi$, corresponding to a δ function interaction between mass patches. In the large κR electrostatic limit discussed above the w_l are constant, so the free energy is proportional to Σ^2. The hydration interaction is also short-ranged, again giving a total interaction roughly proportional to Σ^2. When used to space round capsomeres, these two cases of short-ranged interactions are both equivalent to the large n (short range) limit of Clare and Kepert (1986), and all three yield essentially the same lattices.

The square of the variance of the mass distribution is given by Σ^2 minus the square of the average mass density, so Σ^2 measures what we call "uniform spacing." This differs from the familiar idea of close packing, which fits surfaces together as closely as possible, maximizing van der Waals interactions and tending to produce locally continuous structures. But the global constraint that the close packed, identical MUs must lie on the surface of a sphere inevitably creates fissures or holes, an uneven distribution of mass. Uniform spacing distributes both the mass and the fissures as regularly as the geometry permits, sometimes leading to structures which are actually nowhere locally close packed.

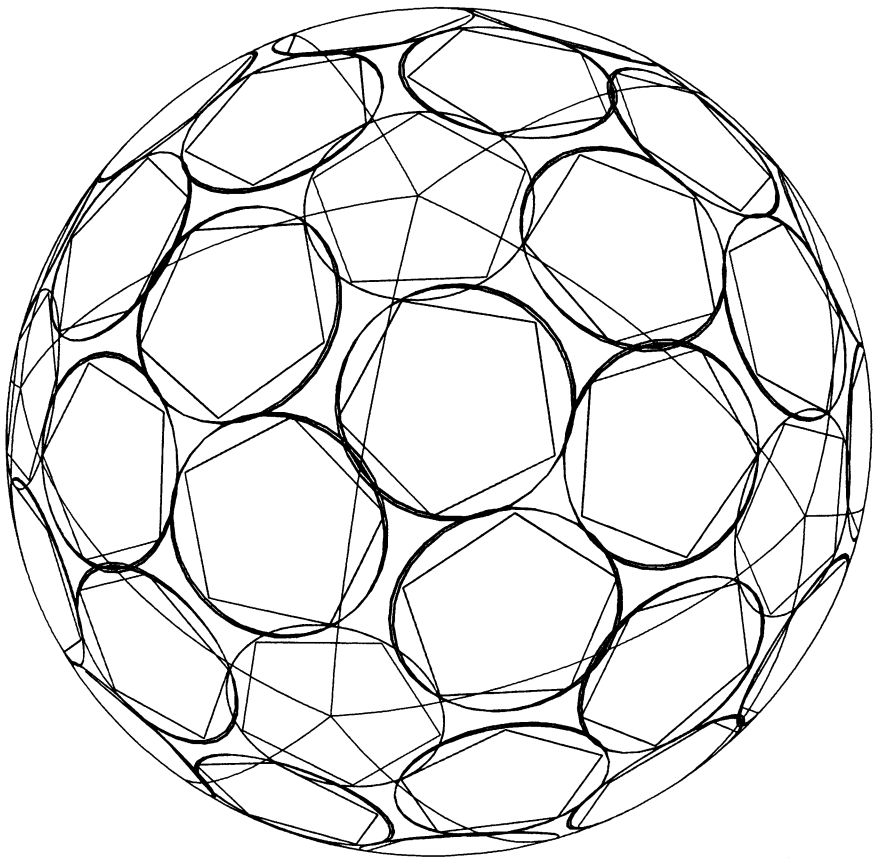

FIGURE 1 Six superimposed $(1, 2)_V$ models; these are made with two interaction functions (δ function and Coulomb potential), applied to each of three kinds of MUs: two disks with Gaussian falloff rates of 0.5 and 1.5, and a pentagon (as used for papilloma and SV40).

The cryoelectron microscopy reconstructions shown below for the papovaviruses are examples of capsids which at most radii are clearly not close packed. By our definition, small MUs placed on a too-large virion might still be packed uniformly, even though large spaces remain between them. Uniform spacing is much easier to assess mathematically than close packing, which is apparent from its appearance in the electrostatic interaction picture.

Both pictures point to the mean square of the surface density, Σ^2, and in fact we might have started there, because Σ^2 is the first moment of a distribution which contains information about its shape. Solutions do not depend strongly on the shape of the w_l curve, as long as it is dominated by local repulsion, and in no cases have we found that a pattern can be significantly "tuned" by adjustments of the w_l. These arguments have led us to set $w_l = 1$ for the bulk of our calculations and to use Σ^2, the measure of uniform spacing, as the measure of capsid pattern fitness.

Modeled with Gaussian radial falloff instead of a hard edge, the MU density never entirely vanishes, so our schematic line drawings show overlap of the nominal edges of the MUs. Because the nominal edge of each MU represents one of its contour levels, any degree of overlap could be eliminated by displaying higher density contours. For consistency, except where noted, the nominal edge contours are chosen as described in the Appendix, but because disks necessarily cover a sphere less neatly than they tile a plane, some overlapping is to be expected. However, since uniform spacing positions the MUs so as to minimize the net overlap, as measured by Σ^2, relative degrees of overlap are significant. In every case, solutions with lower Σ^2 values correspond to schematic figures with smaller overlaps, as judged by eye.

TAXONOMY OF LATTICES

Standard lattices

In practice, we will call two lattices similar if their capsid positions differ by less than a small fraction, say 10%, of the radius of a capsomer. Usually, but not always, we will only need to distinguish among the various sorts of trigonal coordination lattices, because most of the empirically and numerically observed lattices are found to be very like one or another of these. We will call lattices that are similar to the coordination lattices "standard lattices."

The simplest MU is a round Gaussian disk, the parameterization of which is described in the Appendix. Here we note some salient features: the density drops off from unity at the MU center to $1/e$ at its nominal radius, ϕ_R, measured in radians; as a matter of convenience, ϕ_R is chosen so that the MUs cover the sphere with the same efficiency that circles cover a plane, so that a larger value of N means smaller MUs; the Gaussian profile is tuned so that the density falls off most rapidly at the nominal edge of the MU. As seen in Fig. 1, solutions obtained for round, nonstandard Gaussian MUs of differing radii and falloff rates (parameter a in the Appendix) are nearly the same, and this is invariably the case, even for rather unreasonable choices for a and the radius of the disk.

Solutions with MUs located near the vertices of a coordination lattice indexed by integers m and n will be denoted "(m, n) vertex-centered" solutions, or $(m, n)_V$ for short. Because the number of vertices of an (m, n)-coordinated icosahedron is $10T + 2$, an $(m, n)_V$ model uses $N = (10T + 2)$ MUs. In this notation, the $N = 32$ icosahedrally symmetrical packing of Clare and Kepert (1986) is a $(1, 1)_V$ lattice. The vertex-centered solutions are the most efficient ways to pack MUs which are round or nearly round. Fig. 2 shows a raft of vertex-centered (m, n) solutions. In this figure we have outlined each MU at its nominal radius, the radius at which its density is falling off most quickly. The m and n values are found on the abscissa and ordinate axes, respectively, and the radii of the MUs have been chosen as indicated above. The merit of the $(m, n)_V$ solutions in packing disks is clear from inspection, and each $(m, n)_V$ lattice which we have examined is dynamically stable. These structures appear to be close packed, yet essentially the same lattices would be generated by smaller disks, uniformly spaced and noncontiguous, but not close packed.

A second class of standard lattices, which we will call $(m, n)_{V-}$, is obtained by removing the pentonal MU from the vertex-centered lattices. These structures are also dynamically stable. They are a small variation from the $(m, n)_V$ lattices, differing in that the space opened up at the fivefold centers is partly filled by the interior MUs, which simply move over slightly into the newly available space. An $(m, n)_{V-}$ lattice has a larger Σ^2 value than does its $(m, n)_V$ relative. However, between the cases of no pentonal MU and a fully sized one, there exists a family of solutions with pentonal MUs of intermediate size, and the smallest Σ^2 is found when midsized MUs occupy the fivefold centers. This situation may be relevant to virions like adenovirus, which construct the pentonal and interior MUs from different proteins. The $(m, n)_{V-}$ lattices appear in the Tammes problem as well (Tarnai and Gaspar, 1987).

A third, much smaller, class of standard solutions places an MU in the center of each facet of the triangulation lattice, so these are called "facet-centered," denoted $(m, n)_F$. A facet-centered lattice contains $N = 20T$ MUs. Fig. 3 shows several of these, and it is clear that, aside from the $(1, 0)_F$ lattice, they fill space poorly. For round MUs, the facet-centered solutions can be found as extrema for only the smallest values of m and n, even when starting from a good initial guess. The solutions $(1, 0)_F$, $(2, 0)_F$, $(3, 0)_F$, $(4, 0)_F$, $(1, 1)_F$, and $(2, 2)_F$ (along with their mirror images, $m \rightarrow n$ and $n \rightarrow m$) can be found as extrema; but all except $(1, 0)_F$ are unstable. If left to evolve, we see $(1, 1)_F \rightarrow (1, 2)_{V-}$; $(1, 3)_F \rightarrow (3, 3)_{V-}$; $(2, 0)_F \rightarrow (3, 0)_{V-}$; etc.

Because, except for $(1, 0)_F$, they are dynamically unstable, we would not expect to find round facet-centered lattices in nature, unless they relied on an external mechanism to position and stabilize their capsomeres. The facet-centered capsids which do appear in nature have solved the stabilization

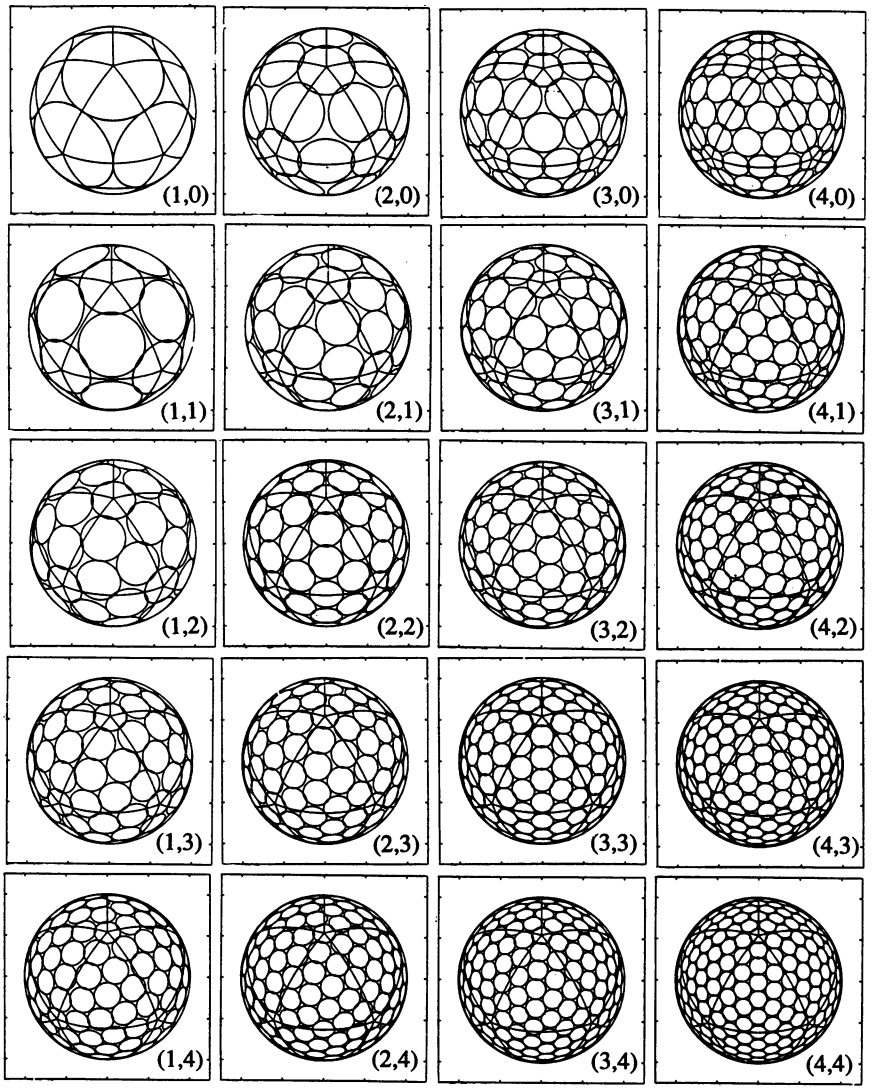

FIGURE 2 Standard vertex-centered $(m, n)_V$ solutions for m = 1–4 (*horizontal axis*) and n = 0–4 (*vertical axis*). The (m, n) solution is a mirror reflection of the (n, m) solution.

problem in various ways, generally by employing decidedly nonround capsomeres. The NβV capsid, discussed below, looks like a $(2, 0)_F$ lattice made of very nonround MUs, stabilized by two sorts of skew.

Nonstandard lattices

We refer to a lattice which is not readily described in terms of a coordination lattice as "nonstandard." Two cases arise; the departure from coordination can be artifactual or structured. When round MUs pack in a nonstandard local minimum, they invariably show a relatively large value of Σ^2 and, if T is large, a large number of local packing arrangements. These patterns typically show concentric bands of badly overlapping MUs centered around the fivefold axes, with large empty spaces in between. Such patterns are an artifact of calculation, not likely representations of actual virions.

The structured nonstandard solutions can occur for substantially nonround MUs. A hint of this is seen in the NβV solution of Fig. 9 *D*, which shows a small skewing of its MUs from the $(2, 0)_F$ lattice. Subsequent work will consider much larger departures from the standard lattices due to nonroundness.

APPLICATIONS TO FOUR VIRUSES

Adenovirus

To illustrate MU dynamics, Fig. 4 shows four different determinations of the same stable $(5, 0)_V$ lattice, the lattice of adenovirus. The trails begin from very similar starting configurations, yet evolve very differently, showing that MU dynamics depend critically on the details, even though the final state does not. These two-dimensional trajectories do not represent the three-dimensional capsid assembly process; but they do demonstrate the stability to tangential perturbations of the final pattern, which is our concern here.

Papilloma

Papilloma belongs to the A genus of the papova family of viruses. It affords an especially interesting application, because cryoelectron microscopy reconstruction shows that the shape of its capsomere protein varies with distance from the virus core (Baker et al., 1991). At radii equal to or greater than 27.0 nm, the capsomere cross-section is star-shaped; at a radius of 25 nm, it is of indistinct symmetry, roughly round; but at 24.1 nm, the cross-section is pentagonal. For a first

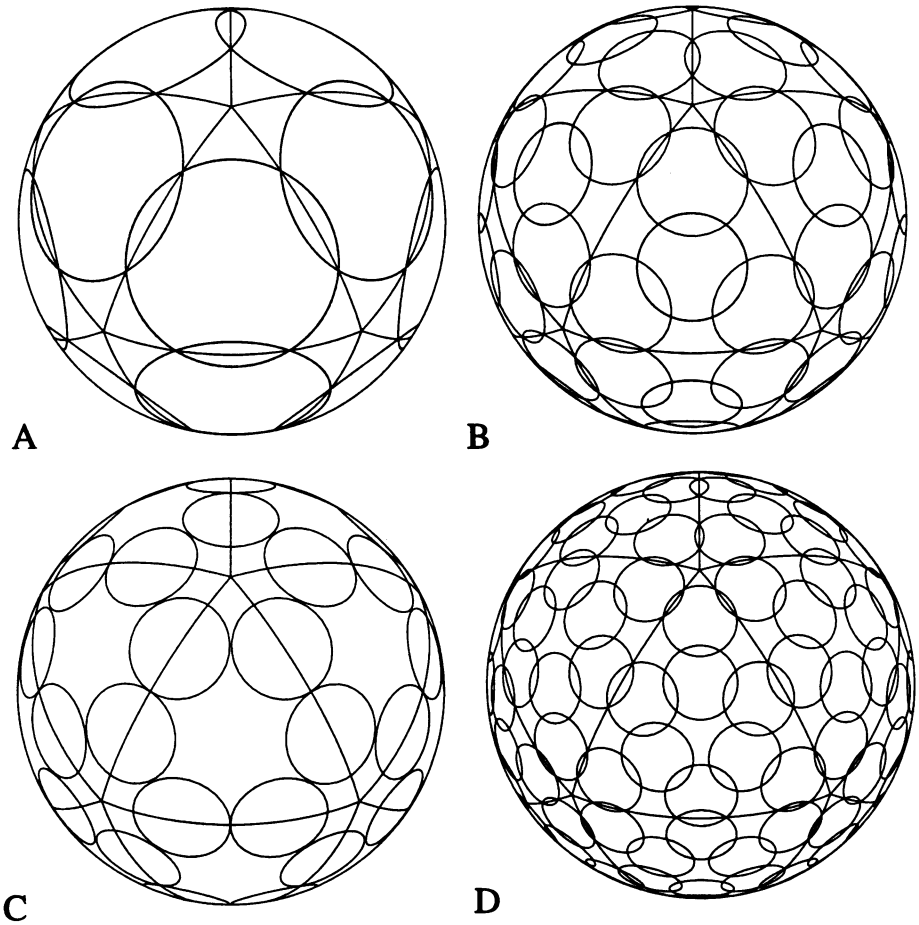

FIGURE 3 Some facet-centered solutions. (*A*) $(1,0)_F$, stable; (*B*) $(2,0)_F$; (*C*) $(1,1)_F$; (*D*) $(3,0)_F$.

approximation to papilloma, we can disregard these shapes and treat the MU as a Gaussian disk. The resulting simple model is the standard $(1,2)_V$ model of Fig. 2, which positions the MUs correctly. This shows that the fivefold symmetry of the papilloma capsomere is not needed to position it, nor are bonding patterns among the capsomeres needed to position them, and that the deviation from roundness at most perturbs the capsomere position from that of the round, standard $(1,2)_V$ model.

But it is of course necessary to include the capsomere shape to model its orientation. Figs. 5 *C* and 6 *C* show the disposition of capsomeres at 27.0 and 24.1 nm, respectively (Baker et al., 1991). The change in the orientation of the capsomere at these two levels has been called a "skew." We have treated these two levels independently, taking as MU the capsomere cross-section at each level. Clearly this approach is feasible only if the results at different levels can easily be reconciled into a smooth capsomere backbone trajectory, and this is in fact what emerges.

Contours for the MUs that we have used to model the star-shaped and pentagon-shaped portions of the capsomere are shown in Figs. 5 *A* and 6 *A*, respectively. The star shape was made by adding a fivefold cosine modulation of amplitude A to a circle of radius R: $r = [R + A\cos(5\phi)]$. By adjusting the amplitude A of the cosine modulation we can make a family of fivefold figures, ranging from circles to starfish shapes. The stars used to model papilloma have a gentle modulation amplitude $A = 0.2$. We have fixed the pentonal MU at the fivefold center, allowing it only one degree of freedom, its orientation angle γ_P. The interior MU has an orientation angle γ_I and two Euler angles, which determine its position, as degrees of freedom. Thus, each level has four degrees of freedom and its own MU shape.

For an overview of what to expect from a complete solution that allows the interior MU to wander freely, we first fixed it at the nominal position determined by the standard $(1,2)_V$ model. This allows exploration of the orientations alone, by calculating Σ^2 as a function of γ_P and γ_I. Fig. 7 *A* shows the Σ^2 contours calculated for the star-shaped MU of Fig. 5 *A*. There are two minima and two maxima, the upper minimum corresponding to the orientation observed for the star-shaped MUs. Fig. 7 *B* shows the contours corresponding to the pentagon-shaped MU of Fig. 6 *A*. Now we find only one minimum, the other having become a shallow shelf. This minimum corresponds to the orientation observed for the pentagon-shaped MUs. It is clear that only one local minimum exists for the pentagon-shaped MUs, but two for the star-shaped MUs. The appearance of the second minimum for the star-shaped MUs is reasonable, given that the star shape has more structure than the pentagon. The maxima occur when the vertices or lobes of the MUs run into each other. The minima represent a policy of avoidance, and for the stars, a sort of knobs-into-holes situation.

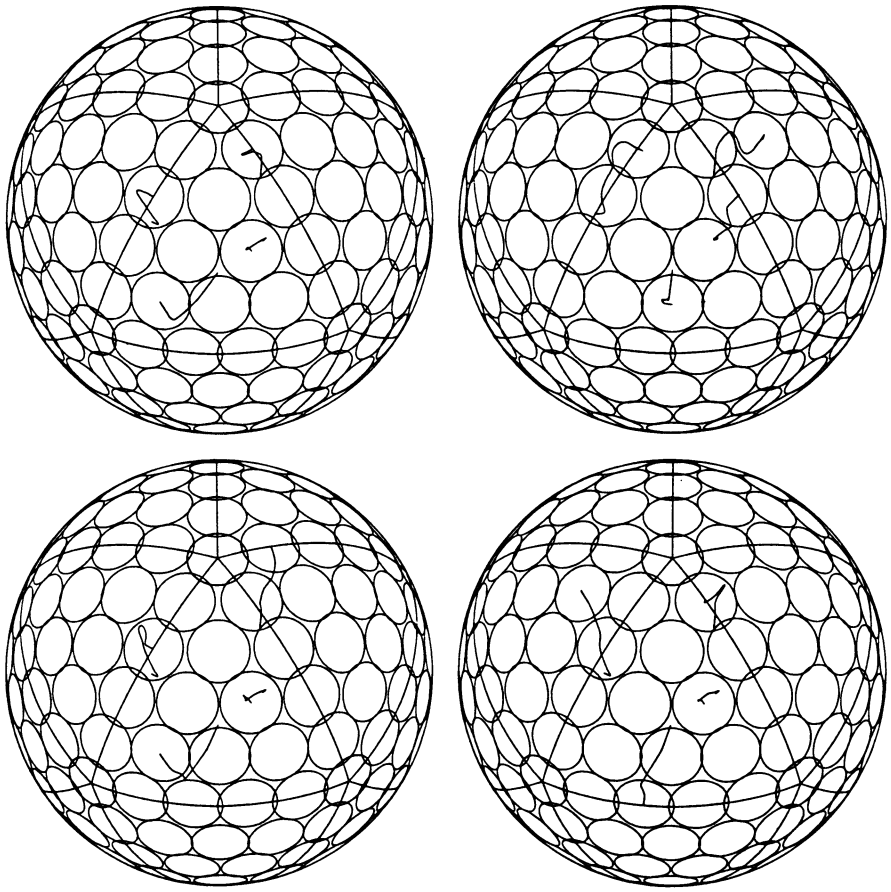

FIGURE 4 Four evolutions to the adenovirus lattice. The trajectories of the independent MUs begin at very similar points but end at different vertices of the standard $(5,0)_V$ lattice.

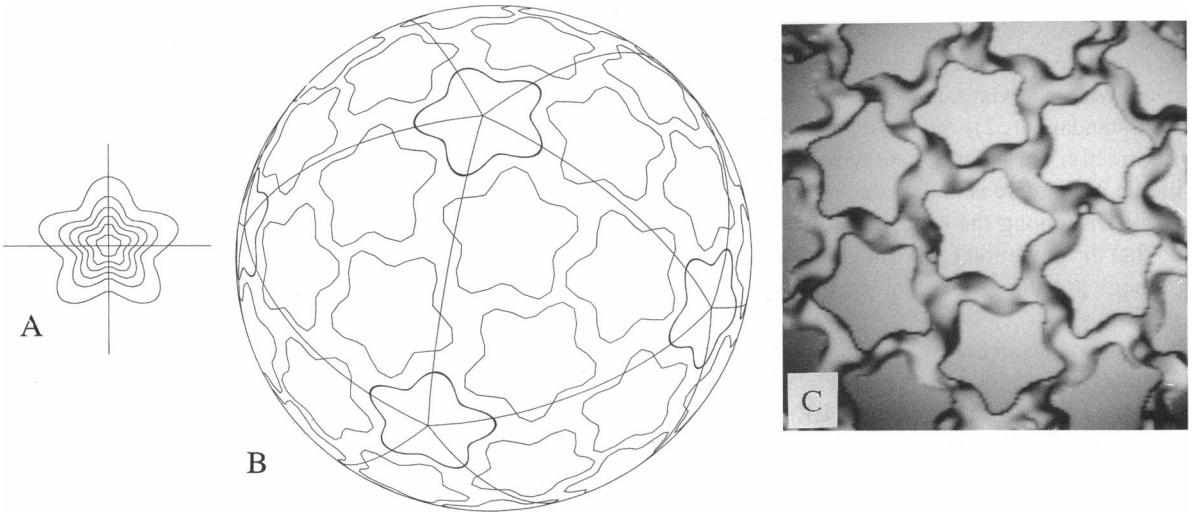

FIGURE 5 Papilloma at 27.0 nm. (*A*) Contours of the modeled MU; (*B*) the local minimum solution for relaxed position of the interior MU and relaxed orientation angles γ_P and γ_I. For comparison with *C*, the contour level chosen to represent the MUs is 0.85 the level of the ,nominal edge of the MU; (*C*) the cryoelectron microscopy reconstruction of the cross-section of papilloma at 27.0 nm radius (Baker et al., 1991).

Figs. 5 *B* and 6 *B* show the final solutions, obtained by minimizing in all four degrees of freedom. The positions have changed only slightly from the nominal $(1, 2)_V$ positions, and the phase angles are represented on the contour plots (Fig. 7) as a star and a pentagon. (They do not lie exactly at the local minima because their positions are not exactly the same as the nominal one used to calculate the contour plots.) Comparison of Fig. 5, *B* and *C*, shows that the fit between the star-like solution and 27.0-nm cross-section is quite close, and Fig. 6, *B* and *C*, compare reasonably well.

The MU positions are close enough in the two solutions that there is no difficulty in supposing that the capsomere axis

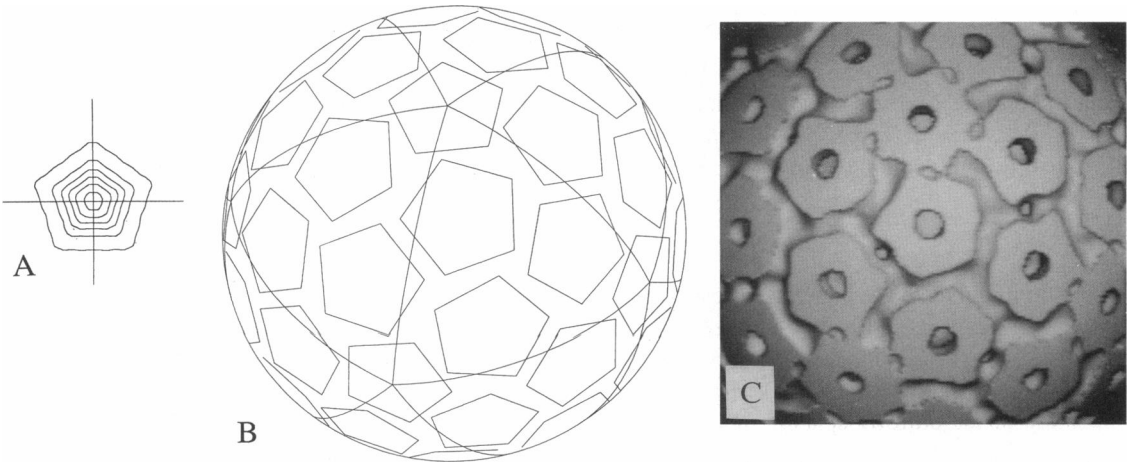

FIGURE 6 Papilloma at 24.1 nm. (*A*) Contours of the modeled MU; (*B*) the local minimum solution for relaxed position of the interior MU and relaxed orientation angles γ_P and γ_I. For comparison with *C*, the contour level chosen to represent the MUs is 0.85 the level of the nominal edge of the MU; (*C*) the cryoelectron microscopy reconstruction of the cross-section of papilloma at 24.1 nm radius (Baker et al., 1991).

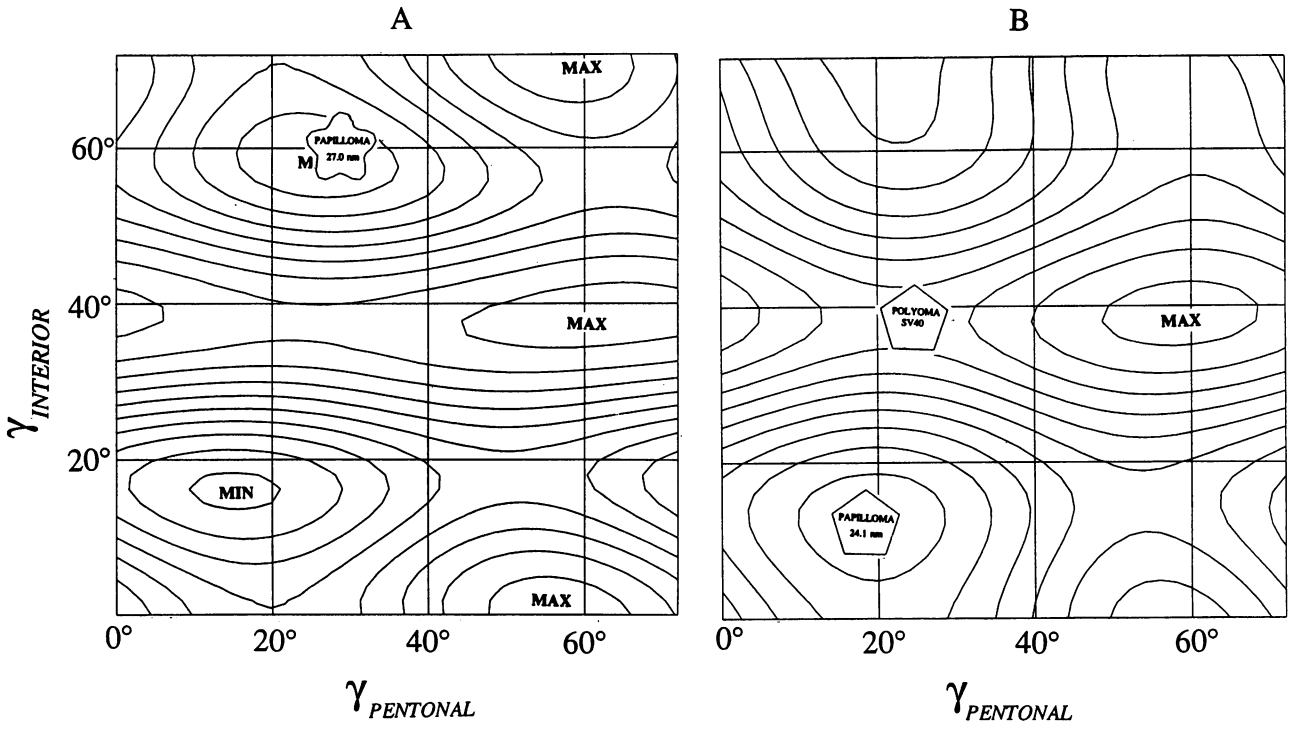

FIGURE 7 Σ^2 contours for papilloma and SV40, with γ_P on the *x*-axis and γ_I on the *y*-axis. Phases are measured counterclockwise; for an MU at the threefold center, zero phase represents a vertex or lobe pointed upward; for an interior MU, zero phase represents the line from the center of the MU through its vertex or lobe pointed toward the threefold center; (*A*) for star-shaped MUs of papilloma at 27.0 nm, two minima exist; (*B*) for pentagonal MUs representing papilloma at 24.1 nm and also SV40, the upper minimum has become a broad shelf. A small star labels the 27.0-nm papilloma model of Fig. 5; a small pentagon labels the 24.1-nm papilloma model of Fig. 6; and a small pentagon at the saddle point labels the SV40 model of Fig. 8.

drifts a bit tangentially as it moves radially. However, the fact that the pentagons choose the lower minimum, whereas the stars choose the upper minimum, raises the question of how the capsomere traverses the high Σ^2 region between the minima in the $\gamma_P - \gamma_I$ plane. The answer is simply that for radii between 24.1 and 27.0 nm, the capsomere cross-section is essentially round, and its orientation does not matter. This contrasts with a possible arrangement which does not occur, wherein the star changes into a pentagon as the cross-section radius decreases, always retaining pronounced fivefold symmetry, and turning through the skew angle along the way. This case would require that the MU traverse the hill between the minima.

The intercapsomere bonding structures, presumably bonding arms much like those of SV40, appear only at the lower radii, where the pentamers are pentagon-shaped. Hints of

them are visible in Fig. 5 *B* between the pentonal pentamers and its neighbors, but they do not appear at the larger radii, where the capsomeres are star-like. The star-like cross-sections orient themselves correctly in our models, without bonding arms; in fact, they agree better with the empirical reconstruction than do the pentameric cross-sections.

SV40

This virus, from the B genus of the papovaviruses, is related to papilloma of the A genus. Baker and co-workers observed that the structural study of the papovaviruses has been marked by "controversy and surprise" (Baker et al., 1989), and our application of the uniform spacing model to SV40 continues in this tradition. Fig. 8, *A* and *B*, shows views down the threefold (Baker et al., 1988) and fivefold (Baker et al., 1989) axes of the cryoelectron microscopy reconstruction of SV40, its $T = 7$ lattice, formed exclusively of pentamers, clearly evident. The corresponding uniform spacing model, using the same pentagonal MU employed for papilloma, is shown in Fig. 8, *C* and *D*. The surprising feature of this model is that it corresponds to the saddle point extremum in Fig. 7 *B*, not to a local minimum. (The other saddle points are unlabeled.)

The saddle point extremum is an unstable equilibrium configuration. At any equilibrium solution, the MUs experience no force tending to displace them. However, unchecked displacements from an unstable equilibrium configuration, in at least one direction, will tend to grow in amplitude, ultimately tending toward a local minimum. At this saddle point, the instability involves only one unstable direction, the orientation angle of the interior MUs, as seen in the contour map. Our interpretation of this arrangement is that the flexible bonding arms of SV40 (Liddington et al., 1991) provide the necessary stabilization to prevent the interior MUs from reorienting themselves, simply by preventing the intercapsomere distance from increasing, which would be necessary if the capsomeres were to reorient. Because the saddle point represents an equilibrium configuration, very little stabilization would be needed, and the mean squared tension on the stabilizing arms would be due only to thermal fluctuations of the structure away from its unstable equilibrium.

Nudaurelia capensis β virus

This virus also shows a skew in the orientation of its morphological units, and NβV is described as having a $T = 4$ surface lattice, with its capsomeres composed of trimers of

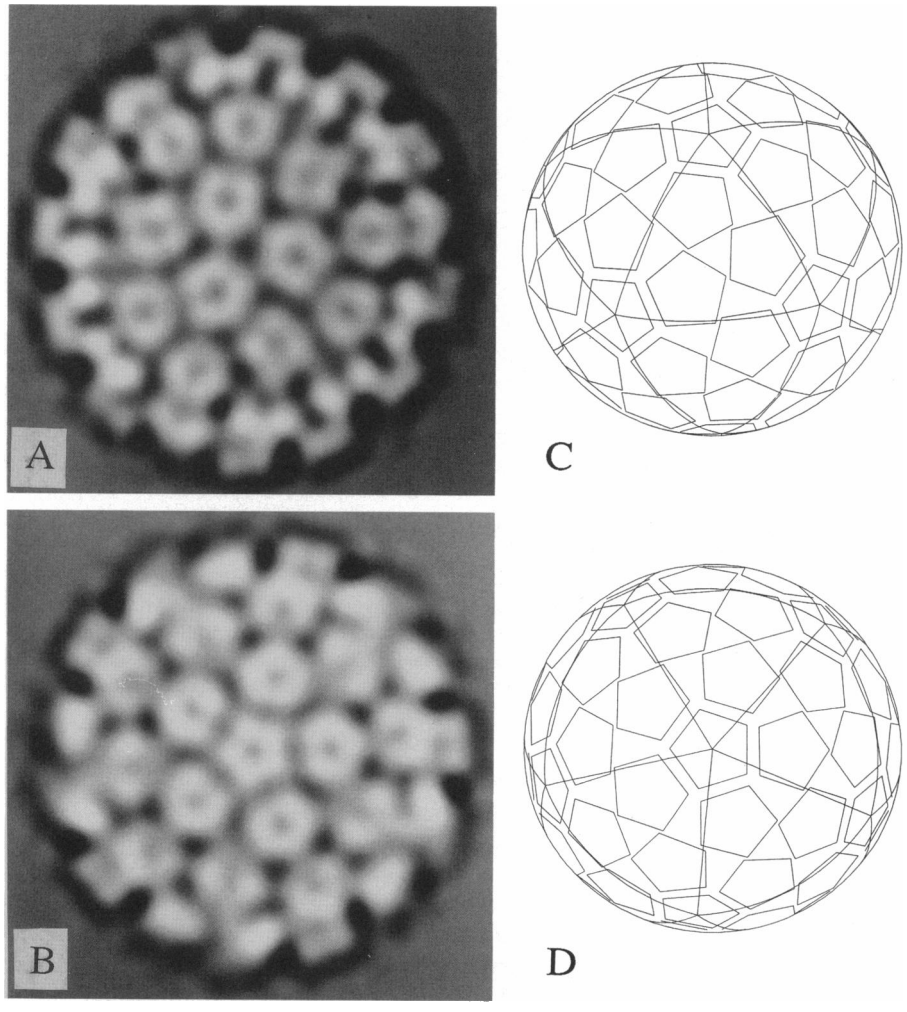

FIGURE 8 (*A*) View down the threefold axis (Baker et al., 1988) and (*B*) view down the fivefold axis (Baker et al., 1989) of the cryoelectron microscopy reconstruction of SV40; *C* and *D* show corresponding views of the saddle point uniform spacing model of SV40 made with the MU of Fig. 6 *A*.

a single subunit (Olson et al., 1990). The capsomeres are located near the centers of facets, rather than at the vertices, the lattice appearing to be $(2, 0)_F$. This is characteristic of irregularly shaped capsomeres, which fill the capsid surface by occupying the centers of the facets of their coordination lattice, rather than its vertices. Fig. 9 *A* shows a cryoelectron microscopy reconstruction of the surface of NβV (Olson et al., 1990); Fig. 9 *B* shows experimental density contours, with the central facet lying in the nominal position and orientation, and the three outlying facets nominally positioned but with their orientation skewed by about 15° clockwise (Olson et al., 1990).

To understand this skew angle, we have modeled NβV, representing its morphological unit by a threefold cosine-modulated circle of amplitude 0.5, as shown in Fig. 9 *C*. The position of one MU is fixed in the center of a face, on the threefold axis, allowing it only one degree of freedom, an orientation angle γ_C. One other, outer, MU possesses the full three degrees of freedom, two position angles, Θ and ϕ, and orientation angle γ_O.

As with papilloma, we first orient ourselves by calculating a contour map (Fig. 10) of Σ^2 as a function of γ_O and γ_C, with the outer MU fixed at the nominal $(2, 0)_F$ position. To the extent that the outer MUs would wander somewhat from this position if allowed to do so, these contours represent approximations only. Orientation angles γ_O and γ_C range between 0° and 120°. Fig. 10 shows two minima, which suggests two solutions, as in the case of papilloma. The lower left minimum corresponds to NβV, and the upper right minimum gives a mirror image capsid. Both minima show skewing from the nominal orientations, which have $\gamma_O = \gamma_C = 60°$. The skew allows the A

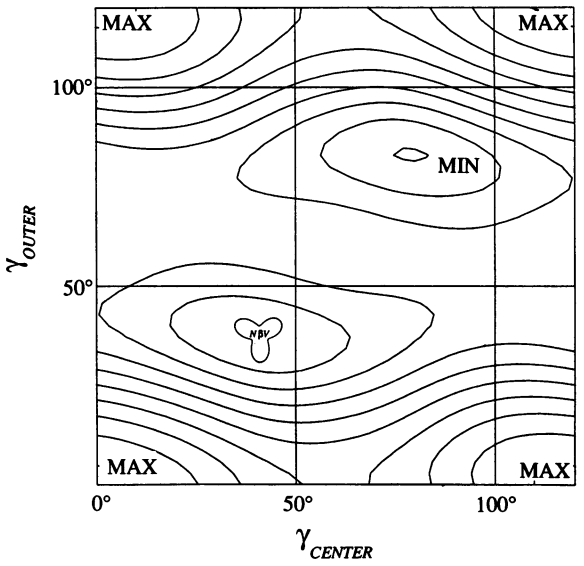

FIGURE 10 Contours of Σ^2 for an NβV type MU modeled as a cosine-modulated circle with amplitude = 0.5. The abscissa is γ_c and the ordinate is γ_o. When $\gamma_o = 0°$, a lobe points toward the threefold axis; $\gamma_c = 0°$ corresponds to the central MU having a lobe pointing upward; phases increase counterclockwise. The solution of Fig. 10 is indicated by the trefoil figure at the minimum.

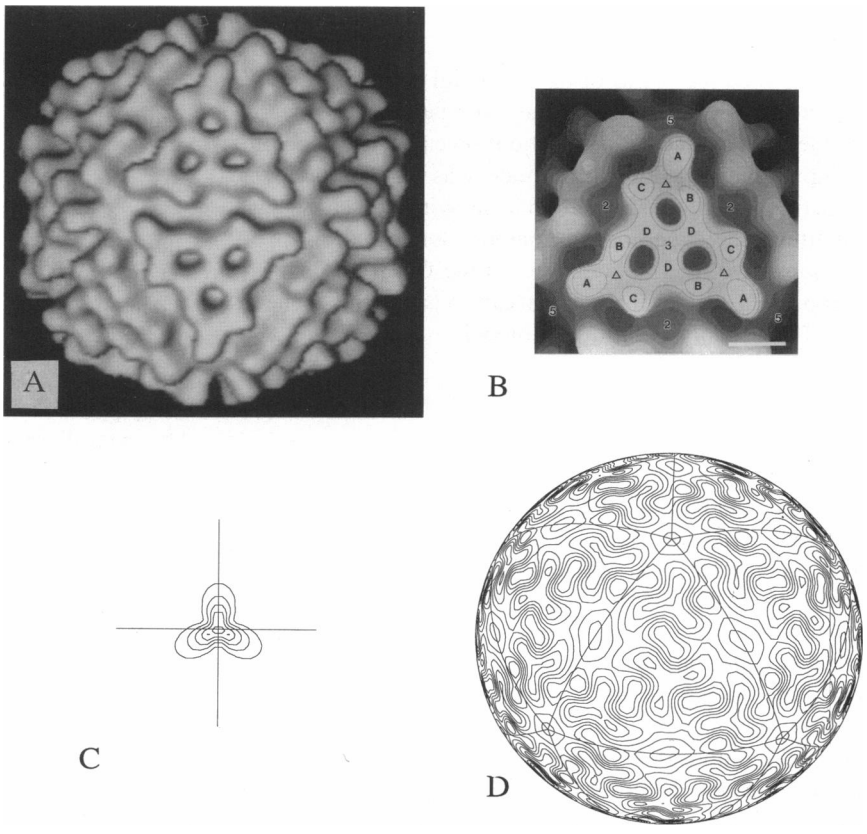

FIGURE 9 (*A*) Experimental reconstruction of the surface of insect virus NβV; (*B*) Experimental contours of insect virus NβV (Olson et al., 1990); (*C*) contours of the MU used to model NβV; (*D*) theoretical contours from the uniform spacing NβV model, which varied γ_o, γ_c, and interior MU position coordinates.

subunits nearest the fivefold centers to avoid each other, atthe expense of a closer contact between the B and D subunits.

By minimizing in all four degrees of freedom, we have found the true minima corresponding to the approximations of Fig. 10, our NβV model. The solution corresponding to the lower minimum has the outer MU positioned very nearly at the nominal $(2, 0)_F$ coordinates. Its face contours are shown in Fig. 9 *D*, which compares well with the experimental contours of Fig. 9 *B*, including the low density regions at the twofold axes and between the local threefold axes and the true threefold axis. The slight skewing of the central MU is not observed by Olson et al. (1990), but we note that it is difficult to orient this MU correctly by observing the icosahedrally symmetric contours of the entire virion.

The NβV solution appears to be a doubly skewed version of a $(2, 0)_F$, $T = 4$ lattice. One skew is in the orientation of the central MU, which shows a 20° clockwise rotation from the "square" orientation. The second skew is a very small rotation of the three outer MUs about the threefold axis, 1.5°, clockwise from the square position. These skews are significant because they show this lattice to be somewhat nonstandard. In subsequent work we will show that this NβV structure belongs to a family of lattices made from cosine-modulated MUs of varying degrees of roundness, some of which stray considerably from the standard lattices. We have found another, nonobserved, solution for the NβV type of MU, in which the outer MU has moved considerably from the positions used to make the contour plot of Fig. 10, rotating clockwise by some 23° from the nominal $(2, 0)_F$ position.

We have modeled NβV with another sort of MU, a trimer built of three equal Gaussian disks. This type of MU is parametrized by the radius of the disks and their separation L. By varying L and the disk radius, we made MUs which resemble the capsomere cross-sections revealed in the contours of Fig. 9 *B*. The resulting NβV model was very similar to that made from cosine-modulated MUs, showing the same skews, and fitting the experimental contours somewhat less well. The success of the model based on the Gaussian disk MU corroborates the idea that a useful capsid pattern model needs only a reasonably faithful MU model.

DISCUSSION

The two-dimensional capsid patterns discussed in this paper were generated by a "bottom-up" strategy, in which the emergent collective behavior of a large number of simple units, interacting in a simple manner, determines a large-scale pattern. The abstractions of capsid taxonomy, such as designations like $(m, n)_{V-}$, for example, are emergent properties not coded into the MUs. A bottom-up strategy contrasts with a "top-down" strategy, which creates a mandated pattern by applying a set of predetermined rules. The top-down approach is more in keeping with an assembly mechanism which builds the pattern, as if from a blueprint, through the actions of enzymes or specific bonding patterns. Bottom-up says how the capsid pattern grows itself, whereas top-down says how it is constructed.

The quasi-equivalence theory (Q.E.) and our uniform spacing approach (U.S.) both explain the observed patterns as extrema of an interaction function, and both consider the relations between the correct number of capsomeres or protein subunits already juxtaposed on a closed shell, but they differ profoundly. Q.E. uses bond deformation energy as the interaction function; U.S. argues that hydration energy and/or electrostatic free energy point to Σ^2. Q.E. generates its capsomeres by clustering protein subunits about the vertex points of the coordination lattice; U.S. inputs its capsomeres and does not try to derive them. Q.E. acts on the local distance scale of covalent bonds; U.S. models interactions on the nanometer scale. Q.E. does not represent the capsomeres mathematically; U.S. uses a continuous representation which allows input of MU shape. Q.E. places its emphasis on the lattices, which are stipulated through a plausibility argument, rather than on the capsomeres; U.S. emphasizes the capsomeres, which are stipulated, and uses capsomere shape to drive dynamic pattern evolution. In short, quasi-equivalence is about the strictly local and specific interactions between protein subunits placed on a lattice, which organizes them into capsomeres, whereas uniform spacing is about longer scaled interactions between preformed capsomeres, which dynamically generate a pattern.

Because of its tendency to blur sharp edges, the Fourier representation is natural for a nanometer resolution scale. This scale length also allows easy access to the connection between the capsomere form and its capsid pattern forming function. The canonical relation between biological form and function, typified by the congruency of enzyme and substrate surfaces, occurs at the atomic distance scale. But the success of the uniform spacing model in reproducing capsid patterns argues that the capsomere fulfills its pattern-forming functions via shapes and interactions characterized on the nanometer, not the atomic, distance scale. Even the flexible bonding arms, a manifest intercapsomere interaction, are functional at the nanometer scale.

The generic nature of the uniform spacing model appears in that the results of the minimization do not strongly depend on what function is chosen for minimization or on the details of the MU modeling. We have argued that a useful and physically plausible function is Σ^2, the average of the square of the mass distribution. Minimization of the electrostatic free energy, calculated via the linearized Poisson-Boltzman equation, and of the hydration energy both point to Σ^2. The standard lattices result inexorably from all nearly round MUs and all interaction functions which are repelling at close range. If the MU shape is made increasingly nonround, departures from the standard lattices are observed, yet the similar NβV models generated from cosine-modulated circles and superimposed Gaussian disk MUs show that even when nonstandard lattices result, the details of the MU modeling are not critical.

Because of shell curvature, each individual capsomere experiences a radial tension which returns it to the capsid

surface should it begin to wander off. The spacing forces, on the other hand, tend to push the capsomeres away from one another, exerting a compression in the tangential direction. In general, such a combination of tensile and compressive forces, as we have posited for the capsid, is characteristic of the "tensegrity" structures, discussed by Buckminster Fuller (1975). He states that "tensegrity provides the ability to yield increasingly without ultimately breaking or coming asunder."

The uniform spacing model is not an assembly model, because it does not produce an icosahedrally symmetrical capsid from capsomeres floating in solution. It treats the compressive, tangential, aspect of a two-force, tensegrity structure (Buckminster Fuller, 1975) as it must exist in equilibrium, after assembly. It assumes that radial, tensile perturbations to the equilibrium have marginal effect on the tangential perturbations with which the model is concerned, that the radial and tangential motions are essentially decoupled normal modes of a three-dimensional linear stability analysis. Corroboration of this assumption must wait until a three-dimensional two-force assembly model is available. For now, it is enough to note that (1) the generic nature of the model suggests that small changes to the interaction function from coupling to radial modes would have marginal effect; (2) the model appears to work without including radial modes. The MU trajectories (e.g., Fig. 4) do not represent the movements of capsomeres as they assemble into a capsid. However, it is likely that MU trajectories representing tangential perturbations from an equilibrium solution do resemble the movements of the outer portions of capsomeres as they undergo small nonradial perturbations. Observed patterns correspond to stable uniform spacing solutions, so until an experimental capsid pattern is found to correspond to an MU configuration with nonvanishing gradients, there is reason to believe that the stability of a uniform spacing pattern to tangential perturbation predicts the stability to equivalent perturbations of the outer portions of the corresponding real capsomeres.

The tangential, compressive, stability of the capsid patterns has been our focus. If external stabilizing interactions are absent, then it is essential that the capsid pattern be dynamically stable, so that small random perturbations from the average capsomere position are damped out. A structure with multiple instabilities (i.e., a global maximum), or one which was not an extremum at all (i.e., at a point in configuration space with non-zero gradient of E_{INT}), would need to be held together entirely by external interactions. Such a structure would not be consistent with the uniform spacing model. The most intriguing situations, intermediate between obvious stability and hopeless instability, involve the saddle point equilibrium structures seen for SV40. The SV40 saddle point possesses a single unstable eigenvalue, so its instability is relatively mild, having only one unstable direction in configuration space and needing stabilization only along this direction; the bonding arms are well-suited for this function. This speculative picture of the role of these nonspecific bonds vis-a-vis capsid stability could be put on firmer ground by comparison among the papovaviruses as structure details become available.

CONCLUSION

We have proved by demonstration that observed capsid patterns, even features like skewing, can be generated without recourse to specific bonds, scaffold structures, or enzyme-mediated mechanisms. This is a step beyond saying that the assembled capsid must be consistent with the shapes of its constituent capsomeres; it suggests that the nanometer scale capsomere geometry determines the nanometer scale capsid architecture. We have argued that the uniform spacing model expresses the tangential stability of a capsid made of capsomeres which interact via both repelling and attractive forces. Thus related to the capsid, the uniform spacing model informs further considerations of capsid architecture, providing a platform from which to proceed. Finally, the model suggests that to assemble into a stable capsid, the capsomeres might need only to be coaxed toward one extremum (usually a local minimum) of a comprehensive free energy function and away from all others, the capsomere shapes directing much of the process.

APPENDIX

The representations of the morphological unit and the capsid

Here we give the details of the representation of the capsid and its self-interaction. The capsid mass distribution is constructed in three steps. First, we write the surface density $\sigma_{\mathrm{MU}}(\Omega)$ of an MU situated at the north pole of a sphere of radius R, where $\Omega \equiv \{\Theta, \phi\}$, a shorthand notation for the usual spherical polar coordinates Θ and ϕ. Second, we write the surface density of a face triangle, $\sigma_{\mathrm{face}}(\Omega)$, containing J MUs located at spherical coordinates $\{\beta_j, \alpha_j\}$ for $j = 1$ to J. (The Θ coordinate is β, and the ϕ coordinate is α.) This is accomplished by rotating σ_{MU} to each of the points (β_j, α_j) and summing the results to form σ_{face}. Third, the surface density of the virion, $\sigma(\Omega)$, is written by rotating σ_{face} to each of the 20 face positions and summing the results.

The first step is an expansion in spherical harmonics:

$$\sigma_{\mathrm{MU}}(\Omega) = \sum_{l=0}^{L} \sum_{m=-l}^{l} a_{lm} Y_{lm}(\Omega), \tag{A1}$$

where the a_{lm} are a set of constant numbers which characterize the shape of the MU. Because all our work is done at a constant radius, the radial coordinate R is suppressed. The spherical harmonics obey the well-known orthogonality relation

$$\delta_{l,l'}\delta_{m,m'} = \int Y_{lm}(\Omega) Y^{*}_{l',m'}(\Omega)\, d\Omega, \tag{A2}$$

where $d\Omega \equiv \sin\Theta\, d\phi\, d\Theta$ is the usual area element in spherical coordinates, and the integral is taken over the entire

spherical surface. Applying Eq. A2 to Eq. A1, we find

$$a_{lm} = \int \sigma_{MU}(\Omega) Y^*_{l,m}(\Omega)\, d\Omega. \quad \text{(A3)}$$

Equation A3 allows us to calculate the a_{lm} corresponding to any assumed σ_{MU}. If the MU is round, then only $m = 0$ terms survive, and if the MU has n-fold symmetry, then a_{lm} is non-zero only if m is a multiple of n.

The second step requires rotating the MU to an arbitrary point on the surface of the sphere, and, once there, rotating it about the local axis. Equation A1 gives an MU located at the north pole, where the local axis $\hat{\eta}$ has spherical coordinates (0, 0). We wish to place an MU at point $\hat{\eta}_j$ with spherical coordinates (β_j, α_j), and then to rotate the MU about axis $\hat{\eta}_j$ by an angle γ_j. Together, these three coordinates are the Euler angles (α_j, β_j, γ_j), which we will denote by the symbol R_j; these angles parametrize the rotation from the standard coordinate system to the primed system, whose z-axis is $\hat{\eta}_j$ (We use the convention of Gottfried (1966), in which the second Euler rotation is about the new y-axis instead of the new x-axis. This allows identification of α_j and β_j with the usual spherical coordinates ϕ_j and Θ_j, respectively.)

The MU rotated by α, β, γ is represented by a new surface density, $\sigma'(\Omega)$, and it is described by a different set of coefficients, a'_{lm}, in the standard coordinate system. However, in the new, primed system, its coefficients a_{lm} will be unchanged. This relationship is written

$$\sigma_{MU}(\Omega') = \sigma'_{MU}(\Omega), \quad \text{(A4)}$$

or

$$\sum_{l=0}^{L} \sum_{m=-l}^{l} a_{lm} Y_{lm}(\Omega') = \sum_{l=0}^{L} \sum_{m=-l}^{l} a'_{lm} Y_{lm}(\Omega). \quad \text{(A5)}$$

Now Ω' represents the spherical coordinates in the primed system. The connection between a spherical harmonic in the coordinate system rotated by (α, β, γ) and those of the standard system is (Gottfried, 1966)

$$Y_{lm}(\Theta', \phi') = \sum_{m'=-l}^{l} Y_{l,m'}(\Theta, \phi) D^l_{m',m}(\alpha, \beta, \gamma), \quad \text{(A6)}$$

where $D^l_{m,m'}$ is a Wigner matrix with the form (Gottfried, 1966; Vogel and Provencher, 1988)

$$D^l_{m,m'}(\alpha, \beta, \gamma) = e^{-im\alpha} d^l_{m,m'}(\beta) e^{-im'\gamma}. \quad \text{(A7)}$$

The matrices $D^l_{m,m'}(\alpha, \beta, \gamma)$ are the lth order representation of the three-dimensional rotation group, acting on basis vectors $Y_{lm}(\Omega)$. The matrix $d^l_{m,m'}(\beta)$ can be calculated by a closed sum (Gottfried, 1966; Vogel and Provencher, 1988) with good accuracy in double precision up to order $l = 50$. Equations A5 and A6 combine to yield

$$a'_{lm} = \sum_{m'=-l}^{l} D^l_{m,m'}(\alpha, \beta, \gamma) a_{l,m'} \quad \text{(A8)}$$

Now in step two we can construct the density of an imaginary face triangle situated at the north pole, composed of a set of J_{face} MUs with Euler coordinates $R_j \equiv (\alpha_j, \beta_j, \gamma_j)$, for $j = 1$ to J_{face}. Summing Eq. A8 over all J_{face} MUs and introducing strengths s_j discussed below, we have

$$\sigma_{face}(\Omega) = \sum_{l=0}^{L} \sum_{m=-l}^{l} b_{lm} Y_{lm}(\Omega), \quad \text{(A9)}$$

where

$$b_{lm} \equiv \sum_{j=0}^{J_{face}} \sum_{m'=-l}^{l} D^l_{m,m'}(R_j) a_{l,m'} s_j. \quad \text{(A10)}$$

The face must have threefold symmetry, so b_{lm} vanishes unless m is a multiple of three. This occurs naturally if all the MUs of the threefold symmetric face are included in the sum over j. However we calculate the same b_{lm} and make a great savings by including only the J dynamically independent MUs, those which are not related to each other by the threefold symmetry; we then set $b_{lm} = 0$ for m not a multiple of three, and multiply the sum over the independent MUs by a factor of three. If an MU is located at the threefold axis, then it requires a strength $s_j = \frac{1}{3}$, lest it be counted three times.

In the third step, we calculate the surface density of the entire capsid:

$$\sigma(\Omega) = \sum_{l=0}^{L} \sum_{m=-l}^{l} c_{lm} Y_{lm}(\Omega), \quad \text{(A11)}$$

so we need to find Fourier coefficients c_{lm}. The surface density of the virion is constructed by rotating the imaginary face at the north pole into the 20 positions occupied by the faces of the icosahedron. Because these 20 faces are situated on the surface of the sphere, they are actually spherical equilateral triangles. For this purpose, we write the matrix

$$I^l_{m,m'} \equiv \sum_{n=1}^{20} D^l_{m,m'}(F_n), \quad \text{(A12)}$$

where $F_n \equiv (\phi_n, \Theta_n, \gamma_n)$ denotes the three Euler angles which parametrize the rotation which carries the imaginary face at the north pole into the nth face of the icosahedron. Then

$$c_{lm} = \sum_{m'=-l}^{l} I^l_{m,m'} b_{l,m'}. \quad \text{(A13)}$$

The matrix $I^l_{m,m'}$ needs to be calculated only once. It is real, and vanishes for $l = 1, 2, 3, 4, 5, 7, 8, 9, 11, 13, 14, 17, 19, 23$, and 29 for $l < 60$. Because the icosahedron has fivefold symmetry, $I^l_{m,m'}$ vanishes unless m is a multiple of five; and the threefold face symmetry requires that b_{lm} vanish unless m is a multiple of three. So, we need to save $I^l_{m,m'}$ only if m' is a multiple of three and m is a multiple of five. It is now clear that if c_{lm} is calculated from Eq. A13, each fivefold vertex is counted five times, and each twofold symmetry point is counted twice. Thus, an MU at a fivefold vertex requires strength $s_j = \frac{1}{5}$, and one at a twofold axis has strength $\frac{1}{2}$.

By defining

$$M^l_{m,m'} \equiv \sum_{j,m''} I^l_{m,m''} D^l_{m'',m'}(R_j) s_j, \tag{A14}$$

we can write finally

$$\sigma(\Omega) = \sum_{l,m,m'} M^l_{m,m'} a_{l,m'} Y_{lm}(\Omega). \tag{A15}$$

In three dimensions, the mass (or charge) density distribution is $\rho(\vec{r}) = \delta(r - R)\,\sigma(\Omega)$, and we normalize so that the total mass (or charge) on the sphere equals the area integral over $\sigma(\Omega)$ or the volume integral over $\rho(\vec{r})$:

$$M \text{ (or } Q) = \int \sigma(\Omega) R^2\, d\Omega = \int r^2\, dr \int d\Omega \rho(\vec{r}) \tag{A16}$$

The interaction function E_{INT}

This formalism can be used to calculate the interaction between the MUs. A fairly general interaction function E_{INT} can be written

$$\begin{aligned} E_{INT} &\equiv \int d^3r_1 d^3r_2 \rho(\vec{r}_1)\rho^*(\vec{r}_2) f(\Phi) \\ &= R^4 \int d\Omega_1 d\Omega_2 f(\Phi)\sigma(\Omega_1)\sigma^*(\Omega_2), \end{aligned} \tag{A17}$$

where Φ is the angle between the axes $\hat{\eta}_1$ and $\hat{\eta}_2$ associated with Ω_1 and Ω_2, respectively, and $f(\Phi)$ is an arbitrary function. This form allows that two patches of the virion surface, at Ω_1 and Ω_2, contribute to the interaction an amount proportional to the product of their surface densities, weighted by a function of the distance between them. To express this in terms of the c_{lm}, we need

$$f(\Phi) \equiv \sum_{l=0}^{L} g_l P_l(\cos\Phi), \tag{A18}$$

which is a standard expansion in terms of Legendre functions; and we need the addition theorem for spherical harmonics (Jackson, 1975):

$$P_l(\cos\Phi) = \frac{4\pi}{(2l+1)} \sum_{m=-1}^{l} Y_{l,m}(\Omega_1) Y^*_{l,m}(\Omega_2). \tag{A19}$$

Combining Eqs. A2, A11, A17, A18, and A19 we find

$$\begin{aligned} E_{INT} &= (4\pi R^4) \sum_{l=0}^{L} \sum_{m=-l}^{l} \frac{g_l}{(2l+1)} c_{lm} c^*_{lm} \\ &= \sum_{l=0}^{L} \sum_{m=-l}^{l} w_l c_{lm} c^*_{lm}, \end{aligned} \tag{A20}$$

where we have introduced $w_l \equiv 4\pi R^4 g_l/(2l+1)$.

The simplest interaction is E_{local}, arising from a purely local, delta function interaction, $f_{local}(\Phi) = \delta(\cos\Phi - 1)$. Inserting this into Eq. A18 and using the completeness relationship for Legendre functions (Jackson, 1975), we find $g_{l,\,local} = (2l+1)/2$ and $w_{l,\,local} = 2\pi R^4$. This can be verified by direct evaluation of Eq. A17.

The average of the square of the mass (or charge) density is given by

$$\Sigma^2 \equiv 1/(4\pi) \int d\Omega \sigma^2(\Omega) = 1/(4\pi) \sum_{l=0}^{L} \sum_{m=-1}^{l} |c_{lm}|^2, \tag{A21}$$

so $E_{local} = \frac{1}{2}(4\pi R^2)^2\, \Sigma^2$.

Linearized Poisson-Boltzmann electrostatics

If we suppose that the MUs carry a charge, then the interaction can be taken as the electrostatic free energy, which we can calculate by means of the linearized Poisson-Boltzmann equation:

$$\nabla^2\phi - (\kappa^2/\epsilon)\phi = -4\pi\rho_a/\epsilon, \tag{A22}$$

where $\rho_a(\vec{r}) = \delta(r - R)\,\sigma(\Omega)$, and is the applied three-dimensional charge distribution, κ^2 is the usual Poisson-oltzmann damping parameter, a constant in this calculation, and ϵ is the dielectric constant, also taken to be constant. We expand the potential field as

$$\phi(\vec{r}) = \sum_{l=0}^{L} \sum_{m=-l}^{l} V_{lm}(r) Y_{lm}(\Omega). \tag{A23}$$

Substituting Eq. A23 and Eq. A11 into A22, and using the completeness relationship Eq. A2 gives the equation for V_{lm}:

$$\begin{aligned} &\left[\frac{\partial}{\partial r} r^2 \frac{\partial}{\partial r} - l(l+1) - \frac{\kappa^2 r^2}{\epsilon}\right] V_{lm}(r) \\ &\qquad = -\frac{4\pi r^2 \delta(r - R) c_{lm}}{\epsilon}. \end{aligned} \tag{A24}$$

The solution is

$$V_{lm}(r) = \frac{4\pi R}{\epsilon} \left(\frac{R}{r}\right)^{1/2} c_{lm} I_{l+1/2}\left(\frac{\kappa r_<}{\sqrt{\epsilon}}\right) K_{l+1/2}\left(\frac{\kappa r_>}{\sqrt{\epsilon}}\right). \tag{A25}$$

Here $r_<$ and $r_>$ are the lesser and greater of r and R, and $I_{l+1/2}$ and $K_{l+1/2}$ denote modified Bessel functions of half-order.

We can now evaluate the Helmholtz free energy A directly:

$$A = \frac{1}{2} \int \rho_a(\vec{r})\phi(\vec{r})\, d^3r. \tag{A26}$$

Substituting for ρ and ϕ, and using the completeness relationship, we find

$$A = \frac{2\pi R^3}{\epsilon} \sum_{l=0}^{L} \sum_{m=-l}^{l} c_{lm} c^*_{lm} I_{l+1/2}\left(\frac{\kappa R}{\sqrt{\epsilon}}\right) K_{l+1/2}\left(\frac{\kappa R}{\sqrt{\epsilon}}\right). \tag{A27}$$

Comparing with Eq. A20 gives

$$w_l = \frac{2\pi R^3}{\epsilon} I_{l+1/2}\left(\frac{\kappa R}{\sqrt{\epsilon}}\right) K_{l+1/2}\left(\frac{\kappa R}{\sqrt{\epsilon}}\right)$$

and

$$g_l = \frac{2l+1}{2R\epsilon} I_{l+1/2}\left(\frac{\kappa R}{\sqrt{\epsilon}}\right) K_{l+1/2}\left(\frac{\kappa R}{\sqrt{\epsilon}}\right).$$

In the large $\kappa R/\sqrt{\epsilon}$ limit, $I_{l+1/2}(x)\ K_{l+1/2}(x) \to 1/2x$ (Jackson, 1975), so we find $g_l \to (2l+1)/4\kappa R^2\sqrt{\epsilon}$, and $w_l = \pi R^2/\kappa\sqrt{\epsilon}$. This interaction is completely local because the w_l are constant, and so in the large $\kappa R/\sqrt{\epsilon}$ limit, we find $A = (4\pi^2R^2)\sum_Q^2/\kappa\sqrt{\epsilon}$, where $\sum_Q^2$, is the average square charge density.

In the small κR limit, $I_{l+1/2}(x)\ K_{l+1/2}(k) \to 1/(2l+1)$ (Jackson, 1975), so we find $g_l \to 1/(2R\epsilon)$, and $w_l = (2\pi R^3/\epsilon)/(2l+1)$. This g_l corresponds (Jackson, 1975) to $f_{\text{Coulomb}}(\Phi) = (1/2\epsilon)/|r_1 - r_2|$, so as $\kappa R\sqrt{\epsilon}$ vanishes, the Coulomb potential is recovered.

Shape of the morphological unit

When we speak of a Gaussian MU of a particular shape, we mean a structure with a surface density given at the north pole by

$$\sigma_{\text{MU}}(\Omega) \equiv e^{-a[\Theta/s(\phi)]^2}. \qquad \text{(A28)}$$

The shape of the MU is determined by $s(\phi)$, which defines the nominal edge of the MU; the parameter a determines the rate of falloff of density with distance from the center of the MU. A disk has $s(\phi) \equiv \phi_R$, a constant which equals the radius of the MU in radians. A pentagon has a ramp function for $s(\phi)$, with $s(\phi + 2\pi n/5) = s(\phi)$. The star-shaped MU used for papilloma has $s(\phi) = \phi_R\ [1 - 0.2\ \cos(5\phi)]$. Each of these shapes is sized to cover the sphere as totally as disks do a plane, covering $\epsilon = \pi/\sqrt{12} = 0.906899$ of its area. For disks, this gives $4\pi\epsilon = 2\pi N(1 - \cos\phi_R)$, for N MUs on the sphere. We have generally set $a = 1$, which makes the MU fall off most rapidly at $\Theta = s(\phi)$. Although the Gaussian MU never falls away to zero, setting $a = 1$ gives an MU with the sharpest "edge."

We are very grateful to T. S. Baker for providing reproductions of results from his laboratory (Figs. 5 *C*, 6 *C*, 8 *A*, 8 *B*, 9 *A*, and 9 *B*). We thank Richard Hendrix and Leondios Kostrikis for helpful discussions.

Financial support through National Institutes of Health grant GM42286-24 is gratefully acknowledged.

REFERENCES

Baker, T. S., J. Drak, and M. Bina. 1988. Reconstitution of the three-dimensional structure of simian virus 40 and visualization of the chromatin core. *Proc. Natl. Acad. Sci. USA.* 85:422–426.

Baker, T. S., J. Drak, and M. Bina. 1989. The capsid of small papova viruses contains 72 pentameric capsomeres: direct evidence from cryo-electron-microscopy of simian virus 40. *Biophys. J.* 55:243–253.

Baker, T. S., W. W. Newcomb, N. H. Olson, L. M. Cowsert, C. Olson, and J. C. Brown. 1991. Structures of bovine and human papillomaviruses. Analysis by cryo-electron microscopy and three-dimensional image reconstruction. *Biophys. J.* 60:1445–1456.

Buckminster Fuller, R. 1975. Synergetics. Macmillan, New York, 369–431.

Burnett, R. M. 1985. The structure of the adenovirus capsid. II. The packing symmetry of hexon and its implications for viral architecture. *J. Mol. Biol.* 185:125–143.

Casjens, S. 1979. Molecular organization of the bacteriophage P22 coat protein shell. *J. Mol. Biol.* 131:1–13.

Casjens, S. 1985. An introduction to virus structure and assembly. *In* Virus Structure and Assembly. S. Casjens, editor. Jones and Bartlett Publishers, Inc., Portola Valley, CA. 1–28.

Caspar, D. L. D., and A. Klug. 1962. Physical principles in the construction of regular viruses. *Cold Spring Harbor Symp. Quant. Biol.* 27:1–23.

Cheng, R. H., N. H. Olson, and T. S. Baker. 1992. Cauliflower mosaic virus: a 420 subunit ($T = 7$), multilayer structure. *Virology.* 186: 655–668.

Clare, B. W., and D. L. Kepert. 1986. The closest packing of equal circles on a sphere. *Proc. R. Soc. Edinb. Sect. A.* 405:329–344.

Dokland, T., B. J. Lindquist, and S. D. Fuller. 1992. Image reconstruction from cryo-electron micrographs reveals the morphopoietic mechanism in the P2-P4 bacteriophage system. *EMBO J.* 11:839–846.

Goldberg, M. 1937. A class of multisymmetric polyhedra. *Tohuku Math J.* 43:104–108.

Gottfried, K. 1966. Quantum Mechanics. W. A. Benjamin, Inc., New York. 287–291.

Harrison, S. C., A. J. Olson, C. E. Shutt, F. K. Winkler, and G. Bricogne. 1978. Tomato bushy stunt virus at 2.9 A resolution. *Nature.* 276:368–373.

Horne, P., and R. W. Wildy. 1961. Symmetry in virus architecture. *Virology.* 15:348–373.

Jackson, J. D. 1975. Classical Electrodynamics. John Wiley and Sons, Inc., New York. 100–102.

Katsura, I. 1983. Structure and inherent properties of the bacteriophage λ head shell. IV. Small head mutants. *J. Mol. Biol.* 171:297–317.

Liddington, R. C., Y. Yan, J. Moulai, R. Sahli, T. L. Benjamin, and S. C. Harrison. 1991. Structure of simian virus 40 at 3.8 A resolution. *Nature (Lond.).* 354:278–284.

Liljas, L., T. Unge, T. Jones, K. Fridborg, S. Lovgren, U. Soglund, and B. Strandberg. 1982. Structure of satellite tobacco necrosis virus at 3.0 A resolution. *J. Mol. Biol.* 159:93–108.

Melnyk, T. W., O. Knop, and W. R. Smith. 1977. Extremal arrangements of points and unit charges on sphere: equilibrium configurations revisited. *Can. J. Chem.* 55:1745–1761.

Olson, A. J., G. Bricogne, and S. C. Harrison. 1983. Structure of tomato bushy stunt virus. IV. The virus particle at 2.9 A resolution. *J. Mol. Biol.* 171:61–93.

Olson, N. H., T. S. Baker, J. E. Johnson, and D. A. Hendry. 1990. The three-dimensional structure of frozen-hydrated *Nudaurelia capensis* β virus, a $T = 4$ insect virus. *J. Struct. Biol.* 105:111–122.

Prevelige, P. E., D. Thomas, and J. King. 1988. Scaffolding protein regulates the polymerization of P22 coat subunits into icosahedral shells *in vitro*. *J. Mol. Biol.* 202:743–757.

Rand, R. P., and V. A. Parsegian. 1989. Hydration forces between phospholipid bilayers. *Biochim. Biophys. Acta.* 988:351–376.

Rau, D. C., and V. A. Parsegian. 1990. Direct measurement of forces between linear polysaccharides xanthan and scizophyllan. *Science (Washington DC).* 249:1278–1281.

Rau, D. C., and V. A. Parsegian. 1992. Direct measurement of temperature-dependent solvation forces between DNA double helices. *Biophys. J.* 61:260–271.

Rayment, I., T. S. Baker, D. L. D. Caspar, and W. T. Murakami. 1982. Polyoma virus capsid structure at 22.5 A resolution. *Nature.* 295:110–115.

Rayment, I. 1985. Animal virus structure. *In* Biological Macromolecules and Assemblies. Vol. 1. F. A. Jurnak and A. McPherson, editors. Wiley-Interscience, New York. 255–298.

Rossmann, M. G., and J. W. Erickson. 1985. Structure and assembly of icosahedral shells. *In* Virus Structure and Assembly. S. Casjens, editor. Jones and Bartlett Publishers, Inc., Portola Valley, CA. 29–73.

Rossmann, M. G., and J. E. Johnson. 1989. Icosahedral RNA virus structure. *Annu. Rev. Biochem.* 58:533–573.

Salunke, D. M., D. L. D. Caspar, and R. L. Garcea. 1989. Polymorphism in the assembly of polymavirus capsid protein VP1. *Biophys. J.* 56: 887–900.

Tammes, P. M. L. 1930. On the origin, number and arrangement of the places of exit on the surface of pollengrains. *Recl. Trav. Bot. Neerl.* 27: 1–84.

Tarnai, T., and Z. Gaspar. 1987. Multi-symmetric close packings of equal spheres on the spherical surface. *Acta Cryst.* Sect. A A43:612–616.

Tarnai, T. 1991. The observed form of coated vesicles and a mathematical covering problem. *J. Mol. Biol.* 218:485–488.

Vogel, R. H., and S. W. Provencher. 1988. Three-dimensional reconstruction from electron micrographs of disordered specimens. II. Implementation of results. *Ultramicroscopy*. 25:223–240.